IEEE Asian Solid-State Circuits Conference
November 5 - 7, 2018/Tainan, Taiwan

# Design of a 2.45-GHz RF Energy Harvester for SWIPT IoT smart sensors

Pengcheng Xu, Denis Flandre and David Bol
ECS group, ICTEAM Institute
Université catholique de Louvain, Belgium
{pengcheng.xu, denis.flandre, david.bol}@uclouvain.be

***Abstract*—Simultaneous wireless power and information transfer (SWIPT) is a flexible and cheap way to supply IoT smart sensors avoiding battery replacement. In this paper, we study the design of a 2.45-GHz RF energy harvester (RFEH) system based on a discrete-component matching network, a custom 65nm CMOS cross-coupled rectifier coupled with an off-the-shelf storage-charging power management unit (PMU) performing rectifier output voltage regulation with maximum power point tracking (MPPT). For 2.45-GHz operation, we propose a parasitic-aware sizing of $\pi$ matching network. This introduces a maximum bound on the real impedance at the rectifier input to ensure good impedance matching in practice. MPPT is used to help reaching this target real impedance at given input RF power, as the rectifier input impedance is a function of both its input and output voltages. Measurement results show a sensitivity as low as -17.1 dBm with a peak power harvesting efficiency (PHE) of 48.3% at -3 dBm 2.45-GHz input RF power. Comparison between simulation and measurement results demonstrate that these results are limited by the parasitic capacitance and that PHE around 45% can be obtained down to -10 dBm with PCB/package improvement for lower parasitic capacitance.**

***Keywords*—RF energy harvester, 2.45-GHz, maximum power point tracking, power harvesting efficiency, impedance matching**

## I. Introduction

Wireless power transfer (WPT) is a flexible way to supply IoT smart sensors without battery replacement. This is usually done with sub-GHz WPT using a specific power transmitter added to the building infrastructure. As mainstream short-range low-power communications like WiFi or BLE uses 2.45-GHz band, sub-GHz WPT also requires a second specific antenna on the smart sensor for receiving the RF power. Therefore, WPT at 2.45-GHz is an interesting alternative for more compact and cheap smart sensors, also re-using BLE/WiFi infrastructure for simultaneous wireless power and information transfer (SWIPT). As an example, such a 2.45-GHz SWIPT occupancy-detection smart system is demonstrated in [1].

Fig. 1 shows a typical RF-supplied IoT smart sensor for SWIPT. The single antenna is used for BLE communications and RF energy harvesting (RFEH). The RFEH system collects the AC electromagnetic power of the RF wireless link and converts it into a DC electrical power to supply the ultra-low-power (ULP) sensor platform. A typical RFEH system is composed of an impedance matching network (MN), an AC/DC rectifier, a power management unit (PMU) and a rechargeable energy storage (battery or supercapacitor). The matching network matches the rectifier input impedance to the antenna impedance, typically 50/75Ω, to avoid reflecting incident RF power. After AC/DC conversion by the rectifier, the PMU generates a stable voltage to supply the ULP platform regardless of the variable incident RF power, while managing the storage element.

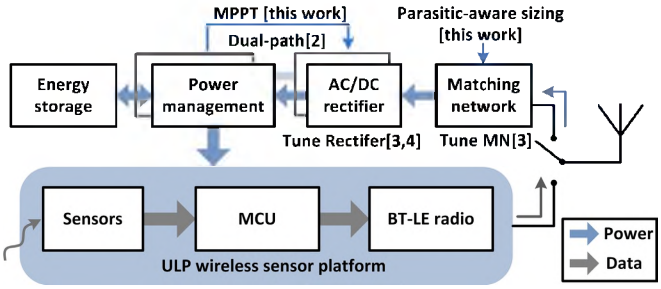


Fig. 1. SWIPT IoT smart sensor and RFEH state-of-art techniques.

Because of strong path loss, the incident RF power is limited in a range from -25 to 0 dBm [1]. Therefore, it is a key challenge for SWIPT system to achieve good harvesting efficiency over this incident power range. Solutions in the literature include dual-path rectifiers, which consists of a low-power path using low-$V_{th}$ transistors for high efficiency at low RF power and a high-power path using high-$V_{th}$ transistors for high efficiency at high input power [2]. Another solution is reconfigurable rectifiers based on multiple identical primary cells connected in series/parallel depending on the input RF power level [3][4]. In order to compensate rectifier impedance variation with input power, a tunable MN based on a capacitor bank was also implemented in [3]. However, in all these solutions, the configuration switches introduce power losses due to their series resistance. Large switches can be selected for low series resistance. However, as we will study in this paper, any parasitic capacitance (e.g. by these switches) added at the rectifier input becomes critical for the MN design at 2.45-GHz. In this paper, we study the design of an RFEH system at 2.45-GHz without reconfiguration switches. We demonstrate the impact of the parasitic capacitance at the rectifier input and validate the interest of rectifier output voltage regulation with maximum power point tracking (MPPT). The proposed RFEH system is presented in Section II. The parasitic-aware sizing of the MN at 2.45-GHz is discussed in Section III. The characteristics of the rectifier operated at its MPPT are studied in Section IV with measurement results in Section V.

978-1-5386-6413-1/18/$31.00 ©2018 IEEE

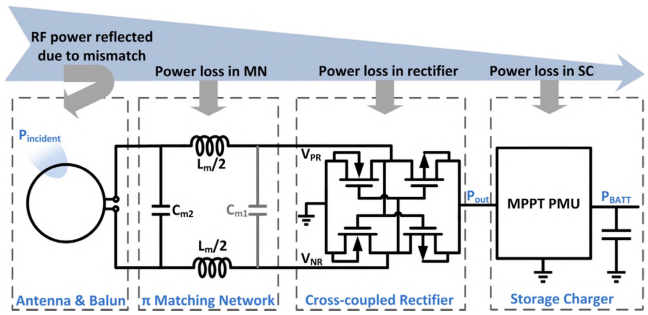


Fig. 2. Proposed RFEH system and its power losses classification.

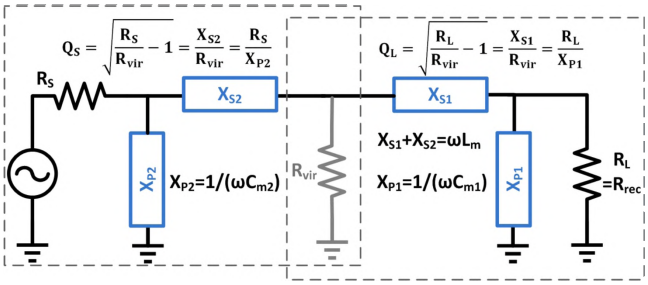


Fig. 3. Π matching network design (the virtual resistor $R_{vir}$ is for sizing but not real component and $R_{vir} \leq \min(R_S, R_L)$).

## II. Proposed RFEH System

The proposed 2.45-GHz RFEH system is depicted in Fig. 2. It is built around a custom cross-coupled rectifier designed in 65nm CMOS. This rectifier architecture allows dynamic self-$V_{th}$ cancellation but as its input is differential, it requires the addition of a Balun to the single-ended antenna. The MN is based on the $\pi$ topology to help cancel the rectifier parasitic input capacitance coming from PCB and chip package, as will be explained in Section III. The rectifier output voltage is regulated by the storage-charging path inside the PMU, which performs MPPT to preserve good power conversion efficiency (PCE) in the rectifier and limit its input impedance variation over the RF incident power range. The PMU also boosts the voltage to charge the storage element.

There are four main sources of RF power losses in RFEH system: RF power reflected back over the air due to impedance mismatch, power loss in the MN, power loss in the rectifier and power loss in the PMU. The power harvesting efficiency (PHE) of RFEH system is the ratio between the extracted DC output power $P_{out}$ delivered to the load (here in Fig. 2 we consider the PMU as the load) and the RF incident electromagnetic power on the receiver antenna, which would be collected with a perfect impedance match, $P_{incident}$ in short. PHE can be expressed as:

$$PHE = P_{BATT}(\text{or } P_{out} \text{ without considering PMU})/P_{incident}.$$

Because of the wide RF incident power range, preserving good PHE over this range is a challenge [1]. Let us mention that the PCE metric defined as $PCE = P_{out}/P_{absorbed} = P_{out}/(P_{incident} - P_{reflected})$ in [5][6] is a limited metric for RFEH systems as it neglects the reflected power due to impedance mismatch. A high PCE is thus a required condition but not a sufficient condition for high performance of RFEH systems. This is why we use the PHE metric as a performance metric in this paper.

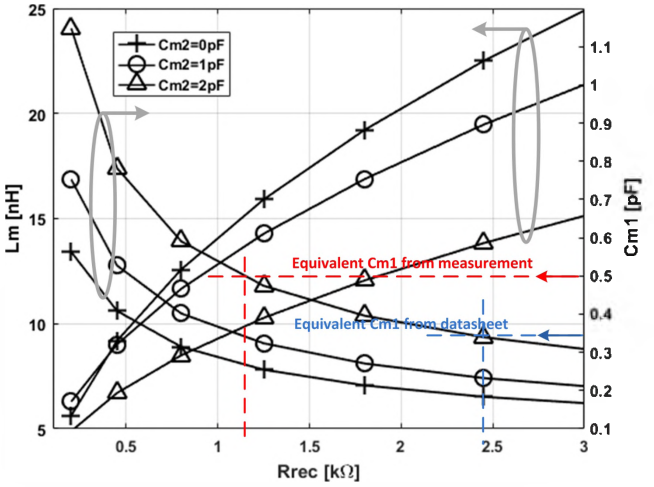


Fig. 4. Sizing of the $\pi$-MN elements vs. $R_{rec}$ at 2.45-GHz with 50-Ω antenna (blue curve with $C_{m1}$=0.35pF and red curve with $C_{m1}$=0.50pF).

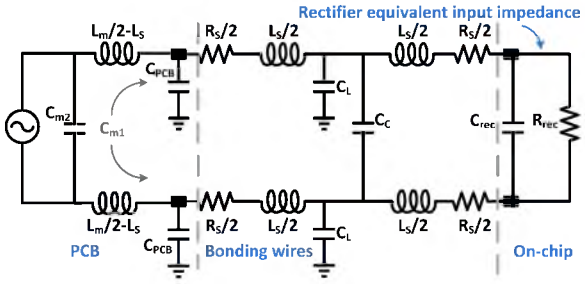


Fig. 5. Model of PCB/package parasitics (5×5mm QFN32L with $R_S$=46mΩ, $L_S$=1.11nH, $C_L$=202fF, $C_C$=39fF).

## III. Parasitic-Aware Sizing of the Matching Network

To extract maximum power from an RF source, the load impedance must be equal to the complex conjugate (i.e. identical real impedance with opposite reactance) of the source impedance. As shown in Fig. 5, the rectifier input impedance $Z_{rec}$ can be modeled as a resistor $R_{rec}$ and capacitor $C_{rec}$ in parallel for representing its real and imaginary parts. In two-element L-MN, the quality factor (Q) is fixed when the source and load impedances are determined. In contrast, $\pi$-MN can be used for narrow-band high-Q application [7]. As described in Fig. 3, it can be separated into two L networks with a virtual resistor $R_{vir}$ whose resistance must be smaller than either antenna impedance $R_S$ or load resistor $R_L$ (here $R_L$ is the input resistance $R_{rec}$ of the rectifier operated at its MPPT) for sizing $\pi$-MN parameters. Fig. 4 shows the required $L_m$ and $C_{m1}$ values to achieve a perfect match as a function of the rectifier input resistance $R_{rec}$ and the $C_{m2}$ value. If $C_{m2}$=0, the $\pi$-MN network is actually an L-MN and the value of its elements $L_m$ and $C_{m1}$ follows the L-MN sizes. Let us mention already that $R_{rec}$ varies with the RF incident power. This comes from the varying voltage amplitude at the rectifier input combined with the highly non-linear characteristics of the transistors at low gate voltage.

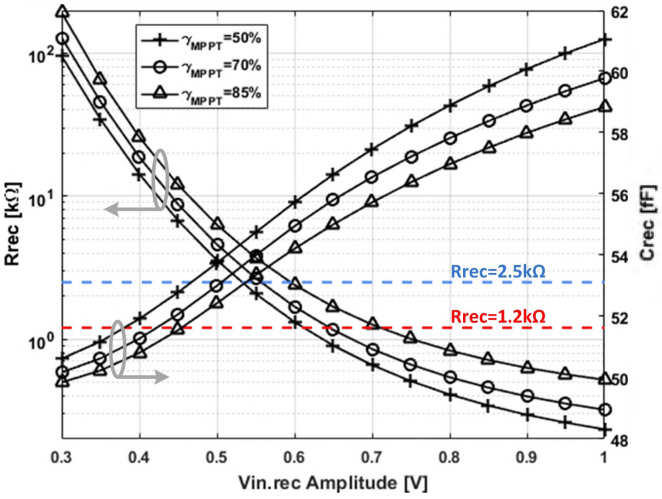


Fig. 6. Rectifier input impedance with four rectifiers in parallel (NMOS 5um/60nm, PMOS 10um/60nm) at 2.45-GHz, $\gamma_{MPPT}=V_{rec.out}/V_{rec.out.OC}$ ($V_{rec.out.OC}$ is $V_{rec.out}$@rectifier output open circuit).

At 2.45-GHz, PCB and package parasitics have a magnified impact compared to sub-GHz. The value of the $C_{m1}$ capacitance in the $\pi$-MN has a minimum value coming from the combination of the PCB ($C_{PCB}$) and package ($C_L$ and $C_C$) parasitics as well as the rectifier equivalent input capacitance ($C_{rec}$). From the datasheet of QFN package model in Fig. 5, the total parasitic from two input RF bonding wires and PCB is around 0.30pF ($=C_L/2+C_C+C_{PCB}/2$) if $C_{PCB}$=0.30pF (with a trace length of 5.5mm and width of 0.7mm in FR4 PCB). Adding $C_{rec}$, $C_{m1}$ minimum value is estimated at 0.35pF. As depicted in Fig. 4, the 0.35pF $C_{m1}$ value requires an equivalent input resistance of the rectifier below 0.5kΩ when $C_{m2}$ is 0pF (corresponding to an L-MN). This is a difficult target for sizing the rectifier at low RF incident power. Therefore, using $C_{m2}$=2pF, the $R_{rec}$ requirement is relaxed to 2.50kΩ. However, in real measurement, due to extra parasitic capacitor from PCB arbitrary soldering and extra bonding wire length for die position, which depends on fabrication technique and is variable case by case, the equivalent $C_{m1}$ is estimated at 0.50pF. The corresponding matched $R_{rec}$ is close to 1.20kΩ with $C_{m2}$=2pF and $L_m$=10nH, which results in an explicit $L_m$ of 7nH considering the parasitic inductance $L_S$ of the bonding wires. This means the best matching occurs when the RF incident power results in an $R_{rec}$ of 1.20kΩ. Let us mention here that assuming sub-GHz WPT at 900MHz, the same 0.50pF $C_{m1}$ equivalent parasitic capacitance would require a target $R_{rec}$ of 4kΩ, which is much easier to obtain at low input RF power.

## IV. Rectifier Characteristic under MPPT Output Voltage Regulation

The proposed RFEH uses a custom rectifier design in 65nm LP CMOS with LVT transistors. It is based on the dynamic self-$V_{th}$-cancellation cross-coupled topology [8], which achieves a higher rectifier PCE than the conventional rectifier, at low input power conditions. In this differential scheme, as shown in Fig. 2, the gate of transistors is actively biased by

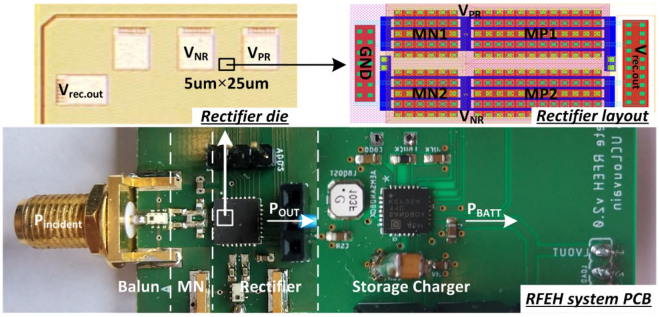


Fig. 7. Proposed RFEH system implementation.

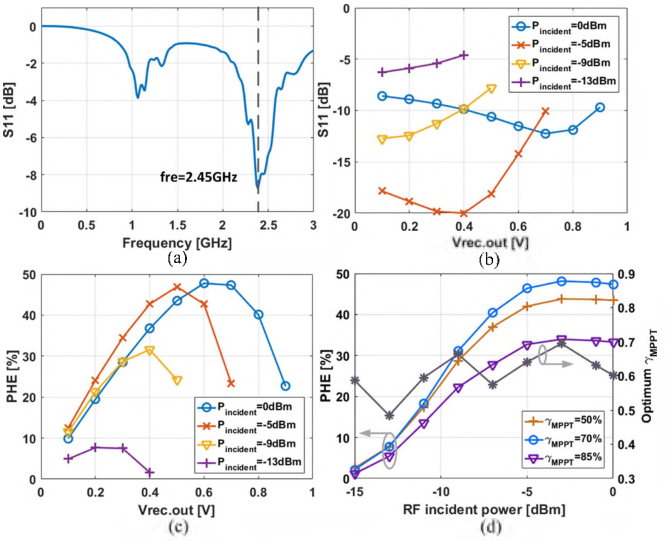


Fig. 8. RFEH measurement results. (a) RFEH operation frequency band. (b) S11 vs. Vout at different input RF power. (c) PHE vs. Vout at different RF input power. (d). Impact of $\gamma_{MPPT}$ ratio on PHE.

a dynamic differential-mode signal. When $V_{PR}$ is negative, which corresponds to the forward bias condition for the MN1 diode, the gate voltage of MN1, which is $V_{NR}$, is positively biased and effectively decreases the turn-on voltage of MN1, resulting in a small ON-resistance. On the other hand, when $V_{PR}$ becomes positive, which corresponds to the reverse bias condition, the gate voltage rapidly decreases, which effectively reduces the reverse leakage current.

For a given sizing of the rectifier, $Z_{rec}$ is a function of the rectifier input $V_{rec.in}$ and output $V_{rec.out}$ voltages as well as the RF frequency:

$$Z_{rec}=R_{rec} \,||\, C_{rec} = f(V_{rec.in}, V_{rec.out}, \text{frequency})$$

Post-layout simulations show in Fig. 6 that, the rectifier input resistance $R_{rec}$ increases greatly at low $V_{rec.in}$ as transistors enter the near-/sub-threshold regime. However, its capacitance $C_{rec}$ is less dependent on rectifier input and output terminal voltage, as the transistor gate capacitance ($C_{gs}$ and $C_{gd}$) variations are cancelled out due to the two differential input voltages $V_{PR}$ and $V_{NR}$.

The selected battery-charging PMU operates with pseudo MPPT. Indeed, it periodically disconnects the rectifier output and senses its open circuit voltage (in this design the $V_{rec.out.OC}$ is close to 0.82 $V_{rec.in}$ amplitude) and then regulates the

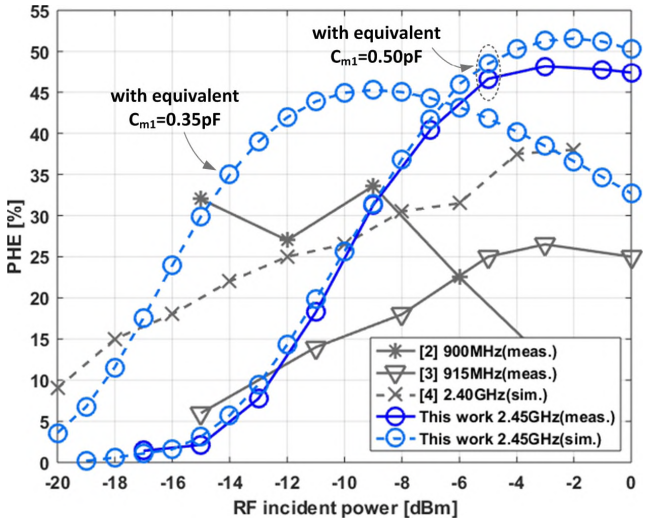


Fig. 9. PHE (=$P_{out}/P_{incident}$ with $\gamma_{MPPT}$=70%) compared to the state-of-art.

rectifier output voltage by forcing $V_{rec.out}$ to a configurable ratio $\gamma_{MPPT}$ of $V_{rec.out.OC}$. Fig. 6 shows that $\gamma_{MPPT}$ affects $R_{rec}$ and the lowest $R_{rec}$ is reached with $\gamma_{MPPT}$ of 50%.

## V. Measurement and Analysis

The cross-coupled RF rectifier was designed and fabricated in 65nm LP CMOS process with 5µm×25µm area. As depicted in Fig. 7, the full RFEH system also includes a Balun, a discrete-component MN and the AEM30940 PMU from e-peas semiconductors for storage charging with pseudo-MPPT. It allows configuring the $\gamma_{MPPT}$ ratio at 50, 70 or 85%.

The measured S11 parameter at the MN input for -5 dBm incident power with open load shows excellent matching at 2.45 GHz as depicted in Fig. 8(a). As this matching depends on $R_{rec}$, it is sensitive to $V_{rec.in}$ and $V_{rec.out}$. Fig. 8(b) shows that optimum matching is reached for different $V_{rec.out}$ values. MPPT thus helps preserving a good matching from 0 dBm to -10 dBm. However, below -10 dBm, the mismatch becomes serious as $R_{rec}$ becomes significantly higher than the target 1.2kΩ for which the MN was sized. Fig. 8(c) clearly shows that the PHE is maximized for a $V_{rec.out}$ voltage that varies from 0.25V to 0.65V as a function of the RF input power. This really validates the need for $V_{rec.out}$ MPPT regulation. The $\gamma_{MPPT}$ ratio to select is analyzed in Fig. 8(d) with the PHE obtained for 50, 70 and 85% ratios. Best PHE is reached at $\gamma_{MPPT}$ ratio of 70% as a trade-off between an optimum PCE at higher $\gamma_{MPPT}$ ratio and a better matching (thanks to lower $R_{rec}$) at lower $\gamma_{MPPT}$.

Fig. 9 show that PHE measurement results are in excellent agreement to the simulation results with all parasitic elements taken into account. The proposed RFEH has excellent performance from 0 dBm to -10 dBm thanks to the parasitic-aware MN sizing methodology and the absence of reconfiguration switches. Below -10 dBm, impedance mismatch shows up. The PHE suffers from both the reflected power loss and the associated $V_{rec.in}$ drop, which results in a low PCE for the rectifier. One 900-MHz RFEH [2] offers a better PHE at low RF incident power, which can be explained by the lower $R_{rec.in}$ requirement at sub-GHz frequency given the parasitic capacitance value (as discussed in Section III). One 2.4-GHz RFEH [4] also obtain slightly better PHE at low $P_{incident}$ but it is based only on simulations without mentioning PCB/package parasitics.

TABLE I. TECHNIQUE AND PERFORMANCE COMPARISON.

| | This work | [2] 2017 TCAS-II | [3] 2017 JSSC | [4] 2016 ISCAS(sim.) |
|---|---|---|---|---|
| **Process** | 65nm | 65nm | 0.18µm | 0.18µm |
| **Frequency** | 2.45GHz | 900MHz | 915MHz | 2.40GHz |
| **Topology** | Cross coupled | Cross coupled | Greinacher doubler | Greinacher doubler |
| **Configuration Switch** | No | Yes | Yes | Yes |
| **Rectifier Load** | MPPT PMU | 147kΩ Resistor | DC/DC Boost | Charged 1V Capacitor |
| **Sensitivity** | -17.1dBm | -17.7dBm | -14.8dBm | -22dBm |
| **Peak PHE** | 48.3% @-3dBm | 34.5% @-9dBm | 26% @-3dBm | 38.4% @-2dBm |

To demonstrate that the PHE of the proposed RFEH system is limited at low $P_{incident}$ by the PCB/chip parasitic capacitance, we simulated the RFEH assuming that this equivalent capacitance could be brought down to 0.35pF. Results in Fig. 9 show that in this case, the PHE can be kept higher than 25% down to -16 dBm with sensitivity below -20 dBm.

## VI. Conclusion

A fully 2.45-GHz RFEH system with MPPT for SWIPT IoT smart sensors is presented in this paper. The proposed π-MN sizing methodology fully considers parasitic components, which are more critical at 2.45-GHz compared to sub-GHz. MPPT helps to improve the PHE by tuning the rectifier input impedance. Measurement results in Table I show a sensitivity of -17.1 dBm and peak PHE of 48.3% at -3 dBm. Simulation shows that reducing the parasitic PCB/package capacitance would result in 45% PHE down to -10 dBm with a sensitivity as low as -22.7 dBm.

## Acknowledgment

This work was supported by the Brussels Institute for Research and Innovation (INNOVIRIS) under the COPINE-IoT project.

## References

[1] R. Dekimpe and et al., "A Battery-less BLE IoT Motion Detector Supplied by 2.45-GHz RF Energy Harvesting," *PATMOS*, 2018.
[2] Y. Lu and et al., "A wide input range dual-path CMOS rectifier for RF energy harvesting," *TCAS-II*, 2017.
[3] M. A. Abouzied and et al., "A fully integrated reconfigurable self-startup RF energy-harvesting system with storage capability," *JSSC*, 2017.
[4] Z. Zeng and et al., "A WLAN 2.4-GHz RF energy harvesting system with reconfigurable rectifier for wireless sensor network," *ISCAS*, 2016.
[5] T. Soyata and et al., "RF energy harvesting for embedded systems: A survey of tradeoffs and methodology," *IEEE Circuits and Systems Magazine*, 2016.
[6] C. R. Valenta and et al., "Harvesting wireless power: Survey of energy-harvester conversion efficiency in far-field, wireless power transfer systems," *IEEE Microwave Magazine*, 2014.
[7] C. Bowick and et al., *RF Circuit Design*, 2nd ed. Newnes, 2008.
[8] K. Kotani and et al., "High-efficiency differential-drive CMOS rectifier for UHF RFIDs," *JSSC*, 2009.